Spin-Selective Oxygen Evolution Reaction in Chiral Iron Oxide Nanoparticles: Synergistic Impact of Inherent Magnetic Moment and Chirality

Aruna Narayanan Nair[†], Sara Fernandez[†], Mariana Marcos[†], Daniel Rascon Romo[‡], Srinivasa Rao Singamaneni [‡], Dino Villagran[†], Sreeprasad Sreenivasan[†]*

†Department of Chemistry and Biochemistry, The University of Texas at El Paso, El Paso, Texas 79968, United States

‡Department of Physics, The University of Texas at El Paso, El Paso, Texas 79968, United States

KEYWORDS: Spin polarization, Oxygen evolution reaction, Chirality induced spin selection, Magnetocurrent

ABSTRACT: Electron spin polarization is identified as a promising avenue for enhancing the oxygen evolution reaction (OER), the bottleneck that limits the energy efficiency of water-splitting. Here, we report that both ferrimagnetic (f-Fe_3O_4) and superparamagnetic iron oxide (s-Fe_3O_4) catalysts can exhibit external magnetic field (H_{ext}) induced OER enhancement, and the activity is proportional to their intrinsic magnetic moment. Additionally, chirality induced spin selectivity (CISS) effect was utilized in synergy with H_{ext} to get a maximum enhancement of up

to 89% improvement in current density (at 1.8 V vs. RHE) with a low onset potential of 270 mV in s-Fe_3O_4 catalysts. Spin polarization and the resultant spin selectivity suppresses the production of H_2O_2 and promote the formation of ground state triplet O_2 during OER. Furthermore, the design of chiral s-Fe_3O_4 with synergistic spin potential effect demonstrates a high spin polarization of ~42%, as measured using conductive Atomic Force Microscopy (c-AFM) measurements.

INTRODUCTION:

According to the principles of quantum theory, the rate of chemical reactions is expected to be sluggish if the spin of the electronic wave function of the products differs from that of the reactants. An archetypal example of this can be seen in a reaction fundamental to many renewable energy devices, namely the OER, where spin conservation is not observed. Here, the reactants -OH/H_2O exist in the singlet spin ground state with no unpaired electrons, while the product O_2 in the ground state is a spin triplet with two unpaired electrons.[1-5] Consequently, quantum mechanics posits that OER is spin-forbidden, requiring additional energy stimuli for the reaction to advance, which contributes to the observed high overpotentials. Although the primary goal of an OER electrocatalyst is to minimize the overpotential for the extraction of electrons with the same spins needed to produce triplet O_2, the significance of the spin attribute was not well recognized until recently.[4, 6] Therefore, despite research efforts to optimize charge transfer at the catalyst interface by modulating band structure of the catalyst, adsorption energies, and electron transport, the issue of high OER overpotentials remains unresolved, potentially due to non-ideal electron spin configurations. Consequently, there has been an increased focus on the "spin transition" at the catalyst interface, aiming to achieve a significant breakthrough in reducing the OER overpotential.[7, 8]

An effective strategy in magnetic catalysts to facilitate selective spin transitions entails imposing spin-dependent potentials that alter the Hamiltonian, leading to the energy band divergence of spin-up and spin-down electrons and subsequently triggering spin polarization. Garcia et al. proposed that an external magnetic field exemplifies a spin-dependent potential that could be harnessed to achieve this objective.[9] Subsequent research has demonstrated that coupling a magnetic field with electrochemistry can better facilitate spin transitions during OER.[9-14] Through quantum exchange interactions, magnetic catalysts can create a lower energy spin-selective channel and transfer electrons of the desired spin to the catalyst-adsorbate interface, thereby boosting OER performance. An alternate pathway to induce spin polarization in catalysts is using chiral molecules.[15, 16] It is documented that the transport of electrons through a chiral molecule can cause spin polarization even in the absence of an external magnetic field (called chirality-induced spin selectivity or CISS effect).[15-19] Thus, chiral molecules can function as spin filters through the CISS effect, selectively transmitting electrons with specific spin orientations and leading to augmented OER kinetics.

Despite advancements, understanding spin polarization mechanisms and the ability to modify them without changing the catalyst's chemical composition/structure is largely unresolved. Specifically, ferromagnetic catalysts can exhibit spin polarization without H_{ext}, and achievable OER enhancement under a H_{ext} is domain size-dependent.[20-22] This finding prompts further exploration of spin polarization phenomena, potentially expanding it to nonferromagnetic catalysts. However, existing research on magnetic field-enhanced electrochemical reactions primarily focuses on single and multi-domain ferromagnetic catalysts, leaving a significant knowledge gap regarding other magnetic catalysts. Unlike ferromagnetic catalysts, superparamagnetic materials do not exhibit inherent spin polarization without H_{ext}.[23] Conversely, the factors influencing spin

polarization in superparamagnetic materials and the combined effects of multiple spin-dependent potentials, such as the co-application of magnetic field and CISS, on enhancing OER activity remain unexplored. Understanding the synergistic impact of such phenomena could unlock strategies to tailor spin polarization in magnetic catalysts, potentially leading to substantially enhanced OER catalysis.

This study investigates the correlation between the intrinsic magnetic properties and the OER activity of nonferromagnetic catalysts, focusing on two types of magnetite catalysts: ferrimagnetic and superparamagnetic. Here, Fe_3O_4 provides an ideal platform for investigating the impact of the magnetic properties of active centers on OER efficiency, as its magnetic properties can be modified without altering chemical composition or structure. Thus, we examine the spin selectivity effect for f-Fe_3O_4 and s-Fe_3O_4 under H_{ext} and decouple various coexisting effects. Furthermore, we introduce the CISS effect into the Fe_3O_4 system by anchoring chiral molecules onto the surface[24-26] and attempt to engineer the total spin polarization in the catalysts through the combined impact of H_{ext} and CISS. The study reveals a significant enhancement, with an 89% improvement in current density at 1.8 V vs. RHE and a low onset potential of 270 mV. The extent of this enhancement intimately ties to the cumulative spin polarization resulting from the intrinsic magnetization in the systems, in conjunction with CISS-induced spin polarization. Spin-selective transport in chiral molecules and ensuing spin polarization are monitored using c-AFM measurements, calculating a spin polarization of up to 42% in the chiral/Fe_3O_4 systems. These findings hold significant implications for the identification of magnetic catalysts and for optimizing the water splitting process through the combined use of different spin potentials such as CISS and H_{ext}.

RESULTS AND DISCUSSION

The f-Fe_3O_4 and s-Fe_3O_4 systems were synthesized following established protocols (see supporting information).[27, 28] Since the synthesis relied on established methods, the resultant samples were characterized primarily to confirm their crystal structure, morphology, and magnetic properties. X-ray diffraction (XRD) spectra (**Figure 1a**) corroborated the inverse cubic spinel crystal structure of both variants, thereby establishing the structural and chemical similarity of the prepared systems.[29, 30] The morphologies were analyzed using scanning electron microscopy (SEM) and transmission electron microscopy (TEM). The SEM images revealed the f-Fe_3O_4 particles as well-defined spheres with an approximate diameter of 200 nm (shown in **Figure 1b**). Conversely, the TEM image of s-Fe_3O_4 (**Figure 1c**) displayed an aggregation of smaller nanoparticles, each less than 50 nm in size (corresponding SEM images in **Figure S1** further affirm the aggregated nature of s-Fe_3O_4). The magnetic properties of the particles were evaluated utilizing vibrating sample magnetometry (VSM) and superconducting quantum interference device (SQUID) measurements. The f-Fe_3O_4 demonstrated ferrimagnetic behavior, with a small remnant magnetization and a mean saturation magnetization of 20 emu g^{-1} (**Figure 1d**), as reported in literature.[31, 32] At room temperature, s-Fe_3O_4 exhibited zero remnant magnetization and a saturation magnetization of 98 emu g^{-1} (shown in **Figure 1e**), which is close to that of bulk magnetite (127 emu g^{-1}). The SQUID measurements, together with the nanoparticle sizes, affirmed the superparamagnetic nature of s-Fe_3O_4.[33-35]

The synthesized nanoparticles with distinct magnetic properties, despite having identical chemical and structural features, are ideal for studying the impact of magnetic properties on spin-selective electrocatalytic OER. The impact of H_{ext} on the electrocatalytic OER activity was evaluated using linear sweep voltammetry (LSV) curves (**Figure S2 a, b**). To exclude the influence of capacitive

background and any anodic oxidation on the OER current, we measured steady-state polarization curves using cyclic voltammetry (CV) (**Figure S3**).

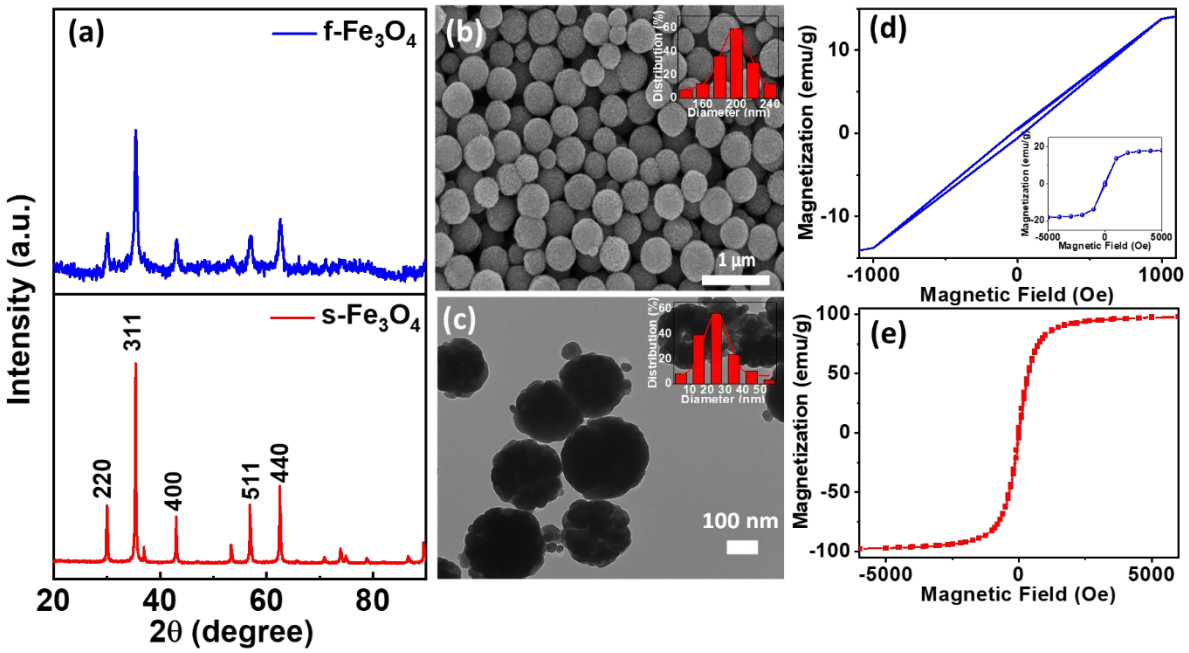

Figure 1: (a) XRD of f-Fe_3O_4 (top) and s-Fe_3O_4 (bottom), (b) SEM image of f-Fe_3O_4, (c) TEM image of s-Fe_3O_4, inset shows corresponding histograms for size distribution (d) Magnetic hysteresis behavior of f-Fe_3O_4, inset shows the hysteresis from -5000 Oe to 5000 Oe (e) Magnetic hysteresis behavior of s-Fe_3O_4

In the absence of H_{ext}, the OER activities of f-Fe_3O_4 and s-Fe_3O_4 were comparable, given their identical Fe active sites and introducing a static H_{ext} enhanced catalytic performance for f-Fe_3O_4 and s-Fe_3O_4. A visible increase in CV currents under H_{ext} of 300 mT for both s-Fe_3O_4 and f-Fe_3O_4 samples confirms the magnetic field-induced enhancement of their OER activities, albeit to different extents. To separate the effects arising from different magnetic properties (while mitigating the influence of surface area differences), the current densities for s-Fe_3O_4 and f-Fe_3O_4 samples were normalized by their respective electrochemical surface areas (ECSA) (calculated following standard protocols; see **Figure S4 and S6**).[36-38] The most significant enhancement under the H_{ext} and the highest activity were observed for s-Fe_3O_4 (with the lowest onset potential of 290 mV vs RHE), as represented by the magnetocurrent densities (j_m) shown in **Figure 2a**. Tafel slope measurements without H_{ext} revealed values close to 120 mV/decade for both samples, suggesting

that the first electron transfer step is the rate-determining step (RDS).[9] However, under H_{ext}, the slope decreased to ~90 mV/decade for f-Fe_3O_4 and s-Fe_3O_4, indicating that the RDS now encompasses a combination of the first and second electron transfer steps (**Figure S2c**).[9] As shown in **Figure 2b and Figure S5**, the overpotential of magnetic Fe_3O_4 samples decreases as the strength of the H_{ext} increases, signifying an acceleration in the OER kinetics. Thus, the promoting effect of H_{ext} on the multi-electron transfer process of OER is more pronounced for the superparamagnetic Fe_3O_4 system. Furthermore, the H_{ext}-induced enhancement maintained stability for up to 24 hours of operation (**Figure S6**).

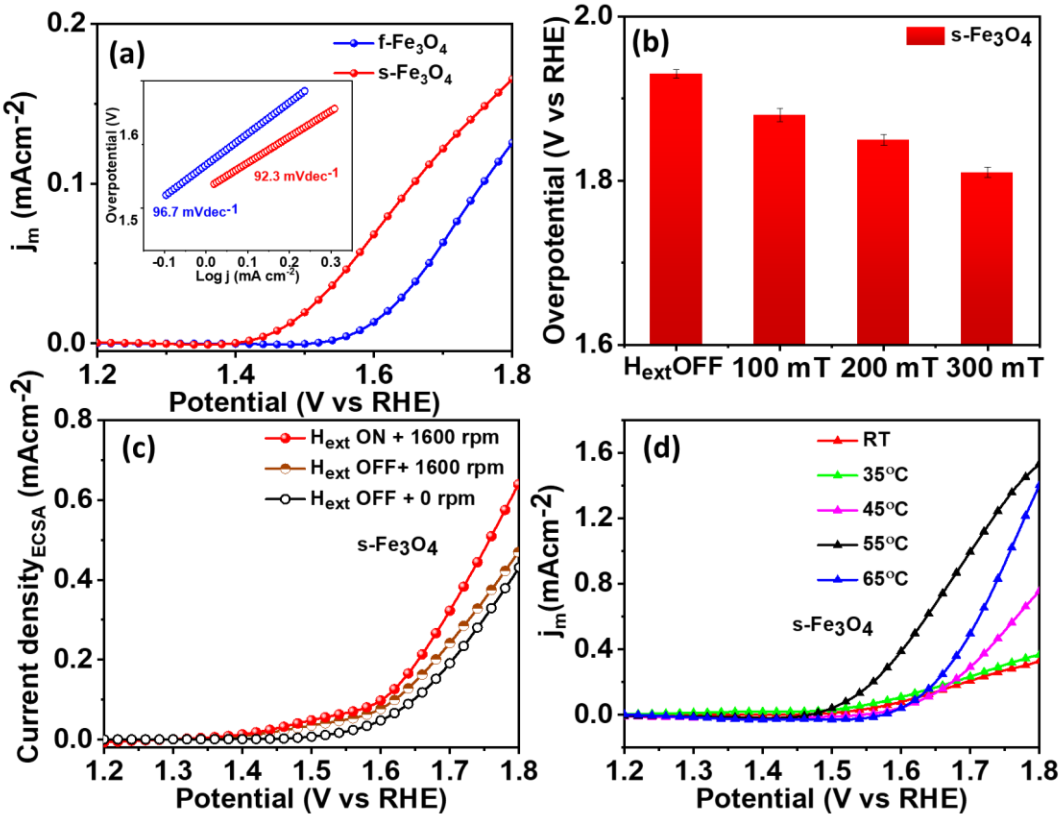

Figure 2: (a) Magnetocurrent density curves for OER (b) Comparison of overpotential for 0.8 $mAcm^{-2}$ at various H_{ext} strengths superparamagnetic Fe_3O_4. (c) Temperature dependence of magnetocurrent in s-Fe_3O_4. (d) stirring and H_{ext} effects in s-Fe_3O_4.

Control experiments were performed to understand the mechanism driving the OER enhancement instigated by H_{ext}. The experiments were designed for discerning the contributions of various

indirect effects and qualitatively isolate the influence of magnetic field-induced spin selectivity. Previous studies have proposed that the magnetohydrodynamic (MHD) effect, can potentially expedite the release of O_2 bubbles, augment mass transfer, and reduce ohmic polarization.[39, 40 41, 42] However, the disparities in the degree of decrease in overpotential observed under the similar H_{ext} for s-Fe_3O_4 and f-Fe_3O_4 suggest that MHD effect is not the sole contributing factor to the improved OER performance. To justify this, the OER activity was measured using a rotating disc electrode (RDE) setup (**Figure 2c**). The slightly elevated OER activity at 1600 rpm can be credited to the enhanced removal of gas bubbles through agitation, while the subsequent increase seen under H_{ext} is attributed to the spin-selection effect.[14] Additionally, ECSA measurements with and without H_{ext} show negligible differences, suggesting minimal impact from the Maxwell stress effect (**Figure S4**).[14] A uniform field strength over the entirety of the small area of the glassy carbon electrode (0.07065 cm^2), effectively eliminates the possibility of the Kelvin force effect influencing the OER measurements.[14] Notably, any influence from magnetic hyperthermia can be disregarded since localized heating occurs only under an alternating magnetic field. Therefore, we surmise that the amplified OER activity under a static H_{ext} originates predominantly from the spin selectivity effect. To further substantiate the above conclusion, we examined the magnetocurrent at various temperatures (**Figure 2d**).[9] The results indicated a decline in magnetocurrent beyond 55^{o}C, potentially due to the disruption of the ferromagnetic ordering in the s-Fe_3O_4 catalysts. This temperature-dependent study emphasized the existence of ferromagnetic ordering under H_{ext} leading to spin polarization and spin selection in s-Fe_3O_4, which augments OER kinetics under magnetic fields. A similar effect of H_{ext} was also observed in f-Fe_3O_4 (**Figure S7**), confirming the spin selectivity effect.

While f-Fe_3O_4 can manifest intrinsic spin polarization without external magnetization,[20, 21] the introduction of H_{ext} triggers domain wall reconstruction, transitioning these into a single domain and consequently boosting OER activity. Conversely, superparamagnetic systems, such as s-Fe_3O_4, require the presence of a H_{ext} to manifest spin polarization, as thermal fluctuations intrinsically disrupt their single-domain magnetizations.[23, 43] Consequently, an improvement in OER activity observed in f-Fe_3O_4 and s-Fe_3O_4 is logical. However, a deeper understanding of the

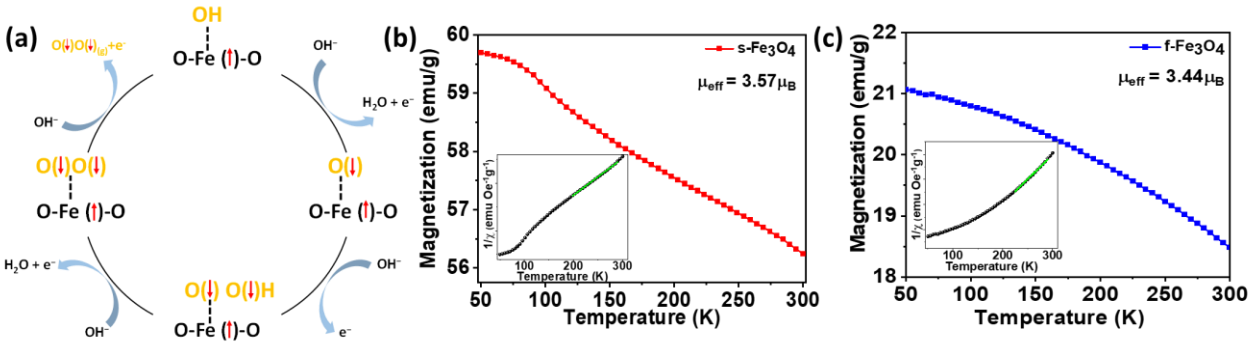

Figure 3: (a) Mechanism of OER under magnetic field and spin selection (b), (c) The field-cooled M-T curves of s-Fe_3O_4 and f-Fe_3O_4, respectively. The inset figure shows the temperature dependence of reciprocal susceptibilities.

origin of the magnetic property is necessary to elucidate the variations between the enhancement. In systems with a fixed total number of electrons, the magnetic moment escalates as the number of spin-up (or spin-down) electrons rises, leading to a higher degree of spin polarization.[9, 44] Therefore, variations in the magnetic moment between samples, leading to resultant differences in effective spin polarization under H_{ext}, could potentially explain the distinct OER activities observed in s-Fe_3O_4 and f-Fe_3O_4. To investigate the potential relationship between magnetic moment and increased spin polarization in Fe_3O_4, we determined the effective magnetic moment (μ_{eff}) from field-cooled M-T curves (**Figures 3c and 3d**). In the high-temperature region, the susceptibilities (χ=M/H) deduced from the magnetizations comply with Curie−Weiss law:

$$\chi = \frac{C}{T} - T_C \qquad (1)$$

where C is the Curie constant, and T_C is the Curie−Weiss temperature. From fitting the susceptibility against temperature data, μ_{eff} was calculated to be 3.57μB for s-Fe_3O_4 and 3.44μB for f-Fe_3O_4, respectively (close to theoretical value 4μB). Based on these findings, it can be inferred that the s-Fe_3O_4 samples, possessing a greater magnetic moment under H_{ext}, exhibit a higher degree of spin polarization leading to a superior spin selectivity effect for OER compared to the f-Fe_3O_4 samples. Building on our comprehension of spin polarization in s-Fe_3O_4, we suggest a mechanism for the spin-polarized OER process, as illustrated in **Figure 3b.** The Fe centers are known to be the OER active sites in Fe_3O_4.[45, 46] Under H_{ext}, the fixed spin direction at Fe active center leads to the generation of $O(\downarrow)^-$, during the first electron transfer step, due to ferromagnetic exchange between the catalyst and the adsorbed oxygen species under the spin angular momentum

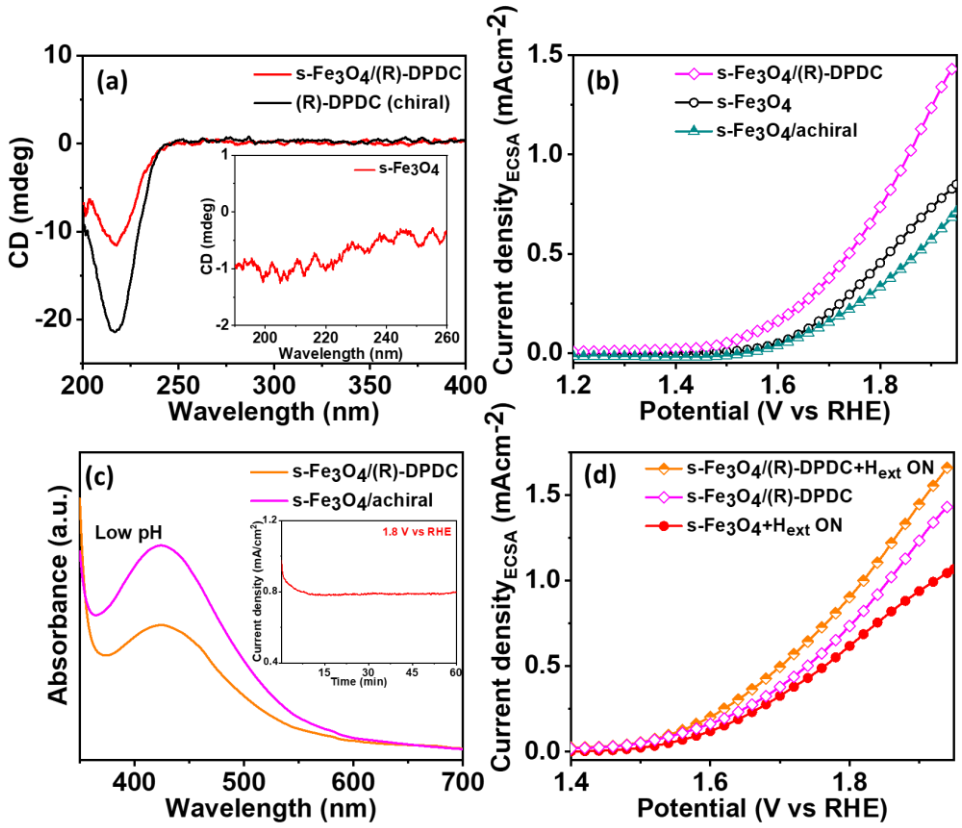

Figure 4: (a) CD measurements (b) LSV polarization curves (c) UV-vis absorption curves for H_2O_2 detection (d) LSV polarization curves for chiral Fe_3O_4 under H_{ext}.

conservation principle.[3, 41] This is followed by subsequent steps with triplet state intermediate O(↓)O(↓)H formation and favorable generation of triplet state O_2.

Having ascertained the crucial role of the inherent magnetic moment of s-Fe_3O_4 in enhancing the OER activity, we sought to further increase spin polarization by introducing an additional spin potential. In light of previous studies highlighting the potential of chiral molecules to enhance OER, [47-49] we anchored chiral molecules directly on the s-Fe_3O_4 surface, thus creating a chiral s-Fe_3O_4 catalyst.[50, 51] The s-Fe_3O_4 system was modified by anchoring both (R) and (S)-1, 2 diaminopropane dihydrochloride [(R)-DPDC and (S)-DPDC], and an achiral molecule, ethylene diamine (ED). The bonding characteristics of all the molecules are the same, allowing us to investigate the influence of chirality on the catalytic properties of s-Fe_3O_4. Circular dichroism (CD) and Fourier transform infrared (FTIR) measurements were utilized to confirm the successful anchoring of chiral molecules. **Figure 4a** demonstrates similar features in the CD spectrum of (R)-DPDC and Fe_3O_4/(R)-DPDC samples, while no CD signal was detected in the spectrum of the s-Fe_3O_4/achiral solution. The presence of chiral features in the CD spectrum confirms the successful attachment of chiral molecules onto the nanoparticles.[50] The corresponding FTIR measurements also endorsed the molecular anchoring on Fe_3O_4 surface (**Figure S8**).

The LSV polarization curves of the chiral samples (**Figure 4b)** indicate that the chiral system exhibits significantly higher OER activity than pristine s-Fe_3O_4 (in the absence of H_{ext}). By comparing the effects of the chiral and achiral systems, it is evident that the improvement in OER activity is directly attributed to the presence of chiral molecules rather than the ligand effects resulting from the bonding of the molecules to the catalyst surface.[52] Interestingly, a minor decrease in activity was observed in the case of s-Fe_3O_4/achiral compared to pristine s-Fe_3O_4, possibly due to the partial blocking of active sites. Interestingly, the chiral system exhibited a 62%

increase in activity, compared to a 43% increase observed for spin selection using H_{ext} (at 1.8 V vs. RHE). These results affirm significance of chiral molecules in enhancing OER. As both the (R) and (S) enantiomers can induce spin-selective electron transfer, no significant difference in the OER enhancement is observed between them (**Figure S9**).

The analysis of H_2O_2 formation as a by-product during OER at low pH revealed that the Fe_3O_4/(R)-DPDC exhibited significant suppression of H_2O_2 production compared to the achiral catalyst (**Figure 4c**). **Figure S10** shows a model lattice representing the polarization of the electron spins of radical intermediates (with blue indicating down spin and grey indicating up spin) on a chiral (spin aligned) and achiral catalyst (random spin) surface. The alignment of the unpaired electrons in two OH radicals can be either antiparallel or parallel. When aligned antiparallel, the reaction occurs on a singlet surface, resulting in the formation of H_2O_2 while hindering the formation of O_2 in its triplet ground state. Conversely, when the spins of the radicals are parallel, the system resides on a triplet potential energy surface, promoting the production of O_2.[53, 54] Notably, in chiral molecules, the antiparallel pathway is suppressed, leading to increased O_2 production. This is consistent with mechanisms proposed in previous reports where the spin-polarized reaction intermediates on chiral catalysts promote the reaction pathway for triplet O_2.[49, 55-59] The cumulative effect of the CISS and H_{ext} on the chiral s-Fe_3O_4 system was investigated, as shown in **Figure 4d**. The combined impact of chirality and magnetic resulted in a higher enhancement (89% increase in current density at 1.8 V vs. RHE) than the individual effects of CISS or H_{ext}. We hypothesize that the chirality and magnetic field contribute two distinct spin-dependent potentials that act in conjunction, increasing spin polarization and overall OER activity.

The spin-dependent charge transport properties of the electrocatalysts were investigated through spin-polarized c-AFM measurements to evaluate the additional spin-dependent potential coming

from chiral molecules. The spin polarization (SP) at a specific electric potential difference, V, is expressed by

$$SP(\%) = \frac{I_{up} - I_{down}}{I_{up} + I_{down}} \, x \, 100 \qquad (2)$$

where I_{up} and I_{down} are the currents measured at a given potential for the magnetic electrode magnetized with the north pole pointing towards the surface or away from it, respectively.[47, 60] **Figure 5a-d** shows the I-V and corresponding spin polarization plots for s-Fe_3O_4/(R)-DPDC and s-Fe_3O_4/(S)-DPDC systems. In s-Fe_3O_4/(R)-DPDC (**Figure 5a)**, the magnetization of the tip in an upward direction has a higher current than the downward direction. The opposite was observed for

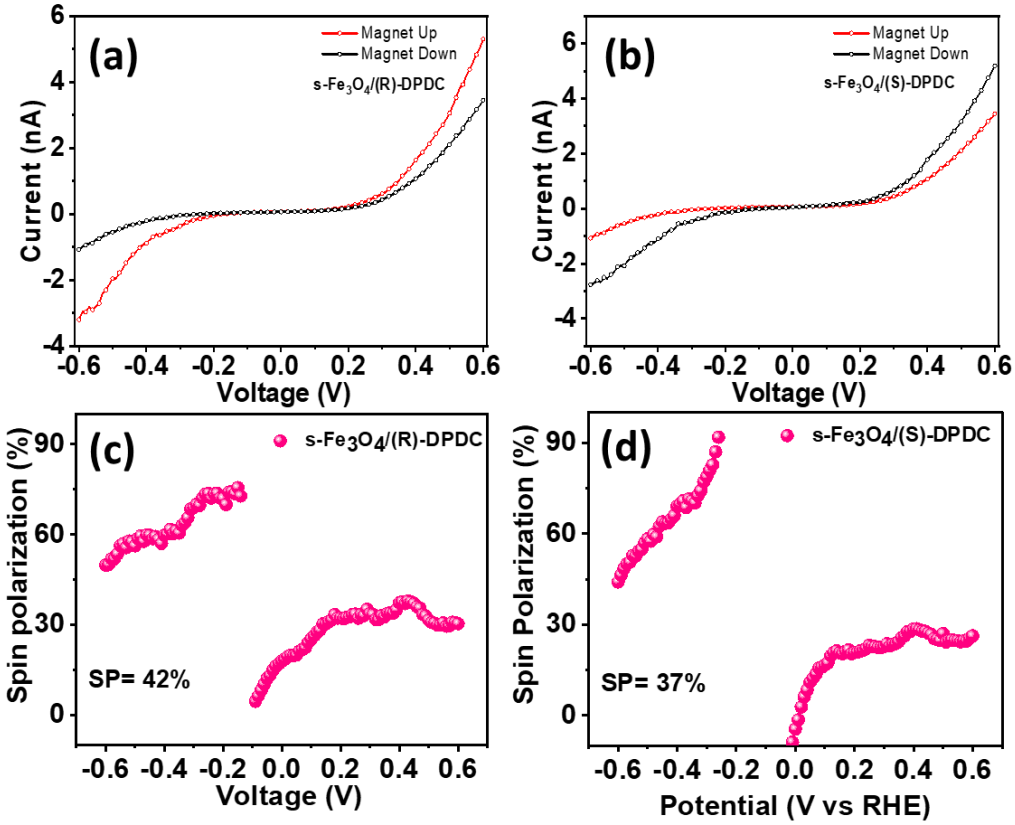

Figure 5: Spin polarization measured with the mc-AFM for (a) s-Fe_3O_4/(R)-DPDC (b) s-Fe_3O_4/(S)-DPDC. Calculated spin polarization as a function of applied bias for (c) s-Fe_3O_4/(R)-DPDC and (d) s-Fe_3O_4/(S)-DPDC.

the s-Fe_3O_4/(S)-DPDC samples (**Figure 5b**), where higher currents were recorded when the tip was magnetized downward. This reveals that the chiral molecules can preferentially select the specific direction of spin-charge carriers and have a different tunneling probability for spin-up and spin-down carriers. The average SP (%) calculated from the c-AFM measurements is 42% for s-Fe_3O_4/(R)-DPDC and 37% for s-Fe_3O_4/(S)-DPDC (**Figure 5c, d)**. Moreover, no considerable changes in the current of the s-Fe_3O_4/achiral sample were observed at different tip magnetization directions (**Figure S11**). The measurements validate the experimental findings, demonstrating the utilization of CISS effect to introduce spin polarization and increase OER activity. Hence, the work opens avenues to combine different spin-dependent potentials to generate synergistic spin polarization and superior OER activities.

CONCLUSIONS

In summary, we have demonstrated the positive synergistic effect of external magnetic field and chiral spin potentials to enhance OER activity. Under H_{ext}, the increase of spatial spin polarization with magnetic moment shows a positive correlation with the enhancement of spin selection during OER. Additionally, our results show that CISS effect can coexist with H_{ext} induced spin polarization to significantly improve OER activity with enhancement up to 89% in current density at 1.8 V vs RHE and low onset potential of 270 mV for s-Fe_3O_4/(R)-DPDC. The spin-polarized electron exchange between the chiral-superparamagnetic Fe_3O_4 and the adsorbed oxygen species under the principle of spin angular momentum conservation, leads to faster reaction kinetics for OER. A maximum spin polarization of 42% was measured using c-AFM in chiral-s-Fe_3O_4. Overall, this study provides valuable insights into the synergistic effects of H_{ext} and the CISS effect, enhancing spin-dependent electrochemical water splitting in hybrid electrocatalysts.

ASSOCIATED CONTENT

Supporting Information.

The following files are available free of charge.

- Experimental details, SEM images of s-Fe_3O_4 nanoparticles, LSV polarization curve and Tafel slopes, CV polarization curve, ECSA for s-Fe_3O_4, Comparison of overpotential at 0.8 $mAcm^{-2}$ under various H_{ext} strengths of f-Fe_3O_4, Stability of s-Fe_3O_4 at 1.8 V vs RHE under Hext, Temperature, stirring and ECSA control measurements on f-Fe_3O_4, FTIR measurements, OER activity of s-Fe_3O_4 with (R) and (S)-DPDC, Mechanistic scheme explaining the role of spin polarization during water splitting, c-AFM measurements for s-Fe_3O_4/achiral sample

AUTHOR INFORMATION

Corresponding Author

Sreeprasad Sreenivasan - *Department of Chemistry and Biochemistry, The University of Texas at El Paso, El Paso, Texas 79968, United States*

Email: sreenivasan@utep.edu

Author Contributions

The manuscript was written through contributions of all authors. All authors have given approval to the final version of the manuscript.

Notes

The authors declare no competing financial interest.

ACKNOWLEDGMENT

S. T. S. acknowledges the primary financial support for the project through DOE grant # DE-FE0031908. A portion of this research was performed at the Center for Integrated Nanotechnologies, which is an Office of Science User Facility operated for the U.S. Department

of Energy (DOE) Office of Science by Los Alamos National Laboratory (Contract 89233218CNA000001) and Sandia National Laboratories (Contract DE-NA-0003525). The authors also acknowledge the utilization of facilities at the Eyring Materials Center at Arizona State University, supported in part of Nanotechnology collaborative Infrastructure (NCI)-Southwest by NSF program NNCI-ECCS-1542160. SRS and DRR acknowledge support from NSF-MRI (Award No. 2018067) and NSF-DMR (Award No. 2105109). D. V thank the Welch Foundation under award number AH-2083-20210327 for providing financial support.

REFERENCES

1. Wu, T.; Xu, Z. J., Oxygen evolution in spin-sensitive pathways. *Current Opinion in Electrochemistry* **2021,** *30*, 100804.
2. Biz, C.; Fianchini, M.; Gracia, J., Strongly correlated electrons in catalysis: focus on quantum exchange. *ACS Catalysis* **2021,** *11* (22), 14249-14261.
3. Li, J.; Ma, J.; Ma, Z.; Zhao, E.; Du, K.; Guo, J.; Ling, T., Spin effect on oxygen electrocatalysis. *Advanced Energy and Sustainability Research* **2021,** *2* (8), 2100034.
4. Sun, Y.; Sun, S.; Yang, H.; Xi, S.; Gracia, J.; Xu, Z. J., Spin-related electron transfer and orbital interactions in oxygen electrocatalysis. *Advanced Materials* **2020,** *32* (39), 2003297.
5. Zhang, Z.; Ma, P.; Luo, L.; Ding, X.; Zhou, S.; Zeng, J., Regulating Spin States in Oxygen Electrocatalysis. *Angewandte Chemie* **2023**.
6. Bai, H.; Feng, J.; Liu, D.; Zhou, P.; Wu, R.; Kwok, C. T.; Ip, W. F.; Feng, W.; Sui, X.; Liu, H., Advances in Spin Catalysts for Oxygen Evolution and Reduction Reactions. *Small* **2023,** *19* (5), 2205638.
7. Li, X.; Cheng, Z.; Wang, X., Understanding the mechanism of the oxygen evolution reaction with consideration of spin. *Electrochemical Energy Reviews* **2021,** *4*, 136-145.
8. Do, V.-H.; Lee, J.-M., Orbital occupancy and spin polarization: from mechanistic study to rational design of transition metal-based electrocatalysts toward energy applications. *ACS nano* **2022,** *16* (11), 17847-17890.
9. Ren, X.; Wu, T.; Sun, Y.; Li, Y.; Xian, G.; Liu, X.; Shen, C.; Gracia, J.; Gao, H.-J.; Yang, H., Spin-polarized oxygen evolution reaction under magnetic field. *Nature Communications* **2021,** *12* (1), 2608.
10. Jiang, S.; Chen, F.; Zhu, L.; Yang, Z.; Lin, Y.; Xu, Q.; Wang, Y., Insight into the catalytic activity of amorphous multimetallic catalysts under a magnetic field toward the oxygen evolution reaction. *ACS Applied Materials & Interfaces* **2022,** *14* (8), 10227-10236.
11. Zhang, Y.; Guo, P.; Li, S.; Sun, J.; Wang, W.; Song, B.; Yang, X.; Wang, X.; Jiang, Z.; Wu, G., Magnetic field assisted electrocatalytic oxygen evolution reaction of nickel-based materials. *Journal of Materials Chemistry A* **2022,** *10* (4), 1760-1767.
12. Li, H.; Liu, S.; Liu, Y., Magnetic enhancement of oxygen evolution in CoNi@ C nanosheets. *ACS Sustainable Chemistry & Engineering* **2021,** *9* (36), 12376-12384.

13. Qin, X.; Teng, J.; Guo, W.; Wang, L.; Xiao, S.; Xu, Q.; Min, Y.; Fan, J., Magnetic field enhancing OER electrocatalysis of NiFe layered double hydroxide. *Catalysis Letters* **2023,** *153* (3), 673-681.
14. Zhang, Y.; Liang, C.; Wu, J.; Liu, H.; Zhang, B.; Jiang, Z.; Li, S.; Xu, P., Recent advances in magnetic field-enhanced electrocatalysis. *ACS Applied Energy Materials* **2020,** *3* (11), 10303-10316.
15. Evers, F.; Aharony, A.; Bar-Gill, N.; Entin-Wohlman, O.; Hedegård, P.; Hod, O.; Jelinek, P.; Kamieniarz, G.; Lemeshko, M.; Michaeli, K., Theory of chirality induced spin selectivity: Progress and challenges. *Advanced Materials* **2022,** *34* (13), 2106629.
16. Wolf, Y.; Liu, Y.; Xiao, J.; Park, N.; Yan, B., Unusual Spin Polarization in the Chirality-Induced Spin Selectivity. *ACS nano* **2022,** *16* (11), 18601-18607.
17. Amsallem, D.; Kumar, A.; Naaman, R.; Gidron, O., Spin polarization through axially chiral linkers: Length dependence and correlation with the dissymmetry factor. *Chirality* **2023**.
18. Meskers, S. C., Consequences of chirality on the response of materials. *Materials Advances* **2022,** *3* (5), 2324-2336.
19. Dalum, S.; Hedegård, P., Theory of chiral induced spin selectivity. *Nano letters* **2019,** *19* (8), 5253-5259.
20. Ren, X.; Wu, T.; Gong, Z.; Pan, L.; Meng, J.; Yang, H.; Dagbjartsdottir, F. B.; Fisher, A.; Gao, H.-J.; Xu, Z. J., The origin of magnetization-caused increment in water oxidation. *Nature Communications* **2023,** *14* (1), 2482.
21. Ge, J.; Ren, X.; Chen, R. R.; Sun, Y.; Wu, T.; Ong, S. J. H.; Xu, Z., Multi-Domain versus Single-Domain: A Magnetic Field is Not a Must for Promoting Spin-Polarized Water Oxidation. *Angewandte Chemie* **2023**, e202301721.
22. Guo, P.; Zhang, Y.; Han, F.; Du, Y.; Song, B.; Wang, W.; Wang, X.; Zhou, Y.; Xu, P., Unveiling the Coercivity-Induced Electrocatalytic Oxygen Evolution Activity of Single-Domain CoFe2O4 Nanocrystals under a Magnetic Field. *The Journal of Physical Chemistry Letters* **2022,** *13* (32), 7476-7482.
23. Bean, C.; Livingston, u. D., Superparamagnetism. *Journal of Applied Physics* **1959,** *30* (4), S120-S129.
24. Fransson, J., Charge redistribution and spin polarization driven by correlation induced electron exchange in chiral molecules. *Nano Letters* **2021,** *21* (7), 3026-3032.
25. Mondal, P. C.; Mtangi, W.; Fontanesi, C., Chiro-Spintronics: Spin-Dependent Electrochemistry and Water Splitting Using Chiral Molecular Films. *Small methods* **2018,** *2* (4), 1700313.
26. Naaman, R.; Paltiel, Y.; Waldeck, D. H., Chiral molecules and the electron spin. *Nature Reviews Chemistry* **2019,** *3* (4), 250-260.
27. Xiong, L. L.; Huang, R.; Chai, H. H.; Yu, L.; Li, C. M., Facile synthesis of Fe3O4@ Tannic Acid@ Au nanocomposites as a catalyst for 4-nitrophenol and methylene blue removal. *ACS omega* **2020,** *5* (33), 20903-20911.
28. Marcos-Hernández, M.; Cerrón-Calle, G. A.; Ge, Y.; Garcia-Segura, S.; Sánchez-Sánchez, C. M.; Fajardo, A. S.; Villagrán, D., Effect of surface functionalization of Fe3O4 nano-enabled electrodes on the electrochemical reduction of nitrate. *Separation and Purification Technology* **2022,** *282*, 119771.
29. ur Rahman, O.; Mohapatra, S. C.; Ahmad, S., Fe3O4 inverse spinal super paramagnetic nanoparticles. *Materials Chemistry and Physics* **2012,** *132* (1), 196-202.

30. Ghaseminezhad, S. M.; Shojaosadati, S. A., Evaluation of the antibacterial activity of Ag/Fe3O4 nanocomposites synthesized using starch. *Carbohydrate polymers* **2016,** *144*, 454-463.
31. Nguyen, M. D.; Tran, H.-V.; Xu, S.; Lee, T. R., Fe3O4 Nanoparticles: Structures, synthesis, magnetic properties, surface functionalization, and emerging applications. *Applied Sciences* **2021,** *11* (23), 11301.
32. Li, Q.; Kartikowati, C. W.; Horie, S.; Ogi, T.; Iwaki, T.; Okuyama, K., Correlation between particle size/domain structure and magnetic properties of highly crystalline Fe3O4 nanoparticles. *Scientific reports* **2017,** *7* (1), 9894.
33. Koo, K. N.; Ismail, A. F.; Othman, M. H. D.; Bidin, N.; Rahman, M. A., Preparation and characterization of superparamagnetic magnetite (Fe3O4) nanoparticles: A short review. *Malaysian J. Fundam. Appl. Sci* **2019,** *15* (1), 23-31.
34. Srivastava, M.; Singh, J.; Yashpal, M.; Gupta, D. K.; Mishra, R.; Tripathi, S.; Ojha, A. K., Synthesis of superparamagnetic bare Fe3O4 nanostructures and core/shell (Fe3O4/alginate) nanocomposites. *Carbohydrate polymers* **2012,** *89* (3), 821-829.
35. Xuan, S.; Wang, Y.-X. J.; Yu, J. C.; Cham-Fai Leung, K., Tuning the grain size and particle size of superparamagnetic Fe3O4 microparticles. *Chemistry of Materials* **2009,** *21* (21), 5079-5087.
36. Nair, A. N.; Sanad, M. F.; Jayan, R.; Gutierrez, G.; Ge, Y.; Islam, M. M.; Hernandez-Viezcas, J. A.; Zade, V.; Tripathi, S.; Shutthanandan, V., Lewis Acid Site Assisted Bifunctional Activity of Tin Doped Gallium Oxide and Its Application in Rechargeable Zn-Air Batteries. *Small* **2022,** *18* (34), 2202648.
37. Nair, A. N.; Sanad, M. F.; Chava, V. S.; Sreenivasan, S. T., Platinum-like HER onset in a GNR/MoS 2 quantum dot heterostructure through curvature-dependent electron density reconfiguration. *Chemical Communications* **2022,** *58* (74), 10368-10371.
38. Sanad, M. F.; Franklin, H. M.; Ali, B. A.; Puente Santiago, A. R.; Nair, A. N.; Chava, V. S.; Fernandez-Delgado, O.; Allam, N. K.; Stevenson, S.; Sreenivasan, S. T., Cylindrical C96 Fullertubes: A Highly Active Metal-Free O2-Reduction Electrocatalyst. *Angewandte Chemie* **2022,** *134* (21), e202116727.
39. Farmani, A. A.; Nasirpouri, F., Boosting hydrogen and oxygen evolution reactions on electrodeposited nickel electrodes via simultaneous mesoporosity, magnetohydrodynamics and high gradient magnetic force. *Journal of Materials Chemistry A* **2020,** *8* (46), 24782-24799.
40. Li, Y.; Zhang, L.; Peng, J.; Zhang, W.; Peng, K., Magnetic field enhancing electrocatalysis of Co3O4/NF for oxygen evolution reaction. *Journal of Power Sources* **2019,** *433*, 226704.
41. Gatard, V.; Deseure, J.; Chatenet, M., Use of magnetic fields in electrochemistry: a selected review. *Current Opinion in Electrochemistry* **2020,** *23*, 96-105.
42. Lin, M.-Y.; Hourng, L.-W.; Wu, C.-H., The effectiveness of a magnetic field in increasing hydrogen production by water electrolysis. *Energy Sources, Part A: Recovery, Utilization, and Environmental Effects* **2017,** *39* (2), 140-147.
43. Mikhaylova, M.; Kim, D. K.; Bobrysheva, N.; Osmolowsky, M.; Semenov, V.; Tsakalakos, T.; Muhammed, M., Superparamagnetism of magnetite nanoparticles: dependence on surface modification. *Langmuir* **2004,** *20* (6), 2472-2477.
44. Choy, T.-S.; Chen, J.; Hershfield, S., Correlation between spin polarization and magnetic moment in ferromagnetic alloys. *Journal of applied physics* **1999,** *86* (1), 562-564.

45. Santos-Carballal, D.; Roldan, A.; Grau-Crespo, R.; de Leeuw, N. H., A DFT study of the structures, stabilities and redox behaviour of the major surfaces of magnetite Fe 3 O 4. *Physical Chemistry Chemical Physics* **2014,** *16* (39), 21082-21097.
46. Righi, G.; Fabris, S.; Piccinin, S., Oxygen evolution reaction on the Fe3O4 (001) surface: theoretical insights into the role of terminal and bridging oxygen atoms. *The Journal of Physical Chemistry C* **2021,** *125* (34), 18752-18761.
47. Bian, Z.; Kato, K.; Ogoshi, T.; Cui, Z.; Sa, B.; Tsutsui, Y.; Seki, S.; Suda, M., Hybrid Chiral MoS2 Layers for Spin-Polarized Charge Transport and Spin-Dependent Electrocatalytic Applications. *Advanced Science* **2022,** *9* (17), 2201063.
48. Feng, T.; Chen, W.; Xue, J.; Cao, F.; Chen, Z.; Ye, J.; Xiao, C.; Lu, H., Spin Polarization of Chiral Amorphous Fe-Ni Electrocatalysts Enabling Efficient Electrochemical Oxygen Evolution. *Advanced Functional Materials* **2023**, 2215051.
49. Im, H.; Ma, S.; Lee, H.; Park, J.; Park, Y. S.; Yun, J.; Lee, J.; Moon, S.; Moon, J., Elucidating the chirality transfer mechanisms during enantioselective synthesis for the spin-controlled oxygen evolution reaction. *Energy & Environmental Science* **2023,** *16* (3), 1187-1199.
50. Zhang, W.; Banerjee-Ghosh, K.; Tassinari, F.; Naaman, R., Enhanced electrochemical water splitting with chiral molecule-coated Fe3O4 nanoparticles. *ACS Energy Letters* **2018,** *3* (10), 2308-2313.
51. Safaei-Ghomi, J.; Zahedi, S., l-Proline-functionalized Fe3O4 nanoparticles as a novel magnetic chiral catalyst for the direct asymmetric Mannich reaction. *Applied Organometallic Chemistry* **2015,** *29* (8), 566-571.
52. Liang, Y.; Banjac, K.; Martin, K.; Zigon, N.; Lee, S.; Vanthuyne, N.; Garcés-Pineda, F. A.; Galán-Mascarós, J. R.; Hu, X.; Avarvari, N., Enhancement of electrocatalytic oxygen evolution by chiral molecular functionalization of hybrid 2D electrodes. *Nature Communications* **2022,** *13* (1), 3356.
53. Naaman, R.; Paltiel, Y.; Waldeck, D. H., Chiral induced spin selectivity gives a new twist on spin-control in chemistry. *Accounts of Chemical Research* **2020,** *53* (11), 2659-2667.
54. Mtangi, W.; Tassinari, F.; Vankayala, K.; Vargas Jentzsch, A.; Adelizzi, B.; Palmans, A. R.; Fontanesi, C.; Meijer, E.; Naaman, R., Control of electrons' spin eliminates hydrogen peroxide formation during water splitting. *Journal of the American Chemical Society* **2017,** *139* (7), 2794-2798.
55. Chrétien, S.; Metiu, H., O 2 evolution on a clean partially reduced rutile TiO 2 (110) surface and on the same surface precovered with Au 1 and Au 2: The importance of spin conservation. *The Journal of chemical physics* **2008,** *129* (7), 074705.
56. Ghosh, K.; Zhang, W.; Tassinari, F.; Mastai, Y.; Lidor-Shalev, O.; Naaman, R.; Möllers, P.; Nürenberg, D.; Zacharias, H.; Wei, J., Controlling chemical selectivity in electrocatalysis with chiral CuO-coated electrodes. *The Journal of Physical Chemistry C* **2019,** *123* (5), 3024-3031.
57. Michaeli, K.; Kantor-Uriel, N.; Naaman, R.; Waldeck, D. H., The electron's spin and molecular chirality–how are they related and how do they affect life processes? *Chemical Society Reviews* **2016,** *45* (23), 6478-6487.
58. Lee, H.; Ma, S.; Oh, S.; Tan, J.; Lee, C. U.; Son, J.; Park, Y. S.; Yun, J.; Jang, G.; Moon, J., Chirality-Induced Spin Selectivity of Chiral 2D Perovskite Enabling Efficient Spin-Dependent Oxygen Evolution Reaction. *Small* **2023**, 2304166.

59. Bhartiya, P. K.; Srivastava, M.; Mishra, D., Chiral-induced enhanced electrocatalytic behaviour of cysteine coated bifunctional Au–Ni bilayer thin film device for water splitting application. *International Journal of Hydrogen Energy* **2022,** *47* (100), 42160-42170.
60. Mondal, A. K.; Preuss, M. D.; Ślęczkowski, M. L.; Das, T. K.; Vantomme, G.; Meijer, E.; Naaman, R., Spin filtering in supramolecular polymers assembled from achiral monomers mediated by chiral solvents. *Journal of the American Chemical Society* **2021,** *143* (18), 7189-7195.

For Table of Contents Only